

DISTINCT NUMERICAL SOLUTIONS FOR ELLIPTIC CROSS-INTERFACE PROBLEMS USING FINITE ELEMENT AND FINITE DIFFERENCE METHODS

QIWEI FENG

ABSTRACT. In this paper, we discuss the second-order finite element method (FEM) and finite difference method (FDM) for numerically solving elliptic cross-interface problems characterized by vertical and horizontal straight lines, piecewise constant coefficients, two homogeneous jump conditions, continuous source terms, and Dirichlet boundary conditions. For brevity, we consider a 2D simplified version where the intersection points of the interface lines coincide with grid points in uniform Cartesian grids. Our findings reveal interesting and important results: (1) When the coefficient functions exhibit either high jumps with low-frequency oscillations or low jumps with high-frequency oscillations, the finite element method and finite difference method yield similar numerical solutions. (2) However, when the interface problems involve high-contrast and high-frequency coefficient functions, the numerical solutions obtained from the finite element and finite difference methods differ significantly. Given that the widely studied SPE10 benchmark problem (see <https://www.spe.org/web/csp/datasets/set02.htm>) typically involves high-contrast and high-frequency permeability due to varying geological layers in porous media, this phenomenon warrants attention. To our best knowledge, so far there is no available literature that has clearly observed such significant differences in the numerical solutions produced by finite element and finite difference methods. Furthermore, this observation is particularly important for developing multiscale methods, as reference solutions for these methods are usually obtained using the standard second-order finite element method with a fine mesh, and analytical solutions are not available. We provide sufficient details to enable replication of our numerical results, and the implementation is straightforward. This simplicity ensures that readers can easily confirm the validity of our findings.

1. INTRODUCTION

Intersecting interface problems arise in many applications, such as the simulation of fluid flow in heterogeneous porous media (see e.g. [1–4, 6, 21, 25, 31, 37, 44, 45]). A well-known example of such a problem is the SPE10 benchmark problem, developed by the Society of Petroleum Engineers (see <https://www.spe.org/web/csp/datasets/set02.htm>). According to [46], the high-frequency permeability in the various geological layers of the SPE10 problem results in a highly oscillatory and high-contrast coefficient function of the interface problem. The singularity of the solution of the intersecting interface problem is notably intensified when the permeability coefficient exhibits substantial discontinuities across interfaces, particularly when these discontinuities span multiple orders of magnitude (see e.g. [5, 7, 18, 26–30, 38, 39, 41, 42]). In this paper, we consider a simplified 2D variant of the elliptic intersecting interface problem, where the interfaces intersect along vertical and horizontal straight lines (see Fig. 1 for an illustration). Since an analytical solution typically does not exist even for this simplified problem, the reference solution is usually obtained by using standard second-order finite element method with linear basis functions and an appropriately fine mesh, such as various multiscale methods (see e.g. [11, 19, 23, 24, 34–36, 43, 50]). However, our numerical results show that FEM and FDM produce markedly different solutions for elliptic intersecting interface problems with high-contrast and highly oscillatory coefficient functions (see Figs. 9 to 12 in Examples 4 to 7).

2010 *Mathematics Subject Classification.* 65N06, 65N30, 35J15, 76S05.

Key words and phrases. Elliptic cross-interface problems, different FEM and FDM solutions, high-contrast and high-frequency coefficients, singularity, the SPE10 benchmark problem.

This research was partially supported by the Mathematics Research Center, Department of Mathematics, University of Pittsburgh, Pittsburgh, PA, USA.

On the other hand, several approaches have been developed to address interface problems with smooth non-intersecting interfaces, piecewise smooth coefficients, two non-homogeneous jump conditions, discontinuous source terms, and mixed boundary conditions. Notable among these are immersed interface methods (IIM, see e.g. [9, 10, 12, 20, 22, 32, 33, 40, 47, 51]), matched interface and boundary (MIB) methods (see e.g. [17, 48, 49, 52, 53]), and sixth-order schemes (see e.g. [13, 14, 16]).

In this paper, we discuss the following elliptic cross-interface problem (see Figs. 1 and 2 for illustrations): *Let the domain $\Omega := (0, 1)^2$. Then we consider:*

$$\begin{cases} -\nabla \cdot (a \nabla u) & = f \quad \text{in } \Omega \setminus \Gamma, \\ [u] & = 0 \quad \text{on } \Gamma, \\ [a \nabla u \cdot \vec{n}] & = 0 \quad \text{on } \Gamma, \\ u & = 0 \quad \text{on } \partial\Omega, \end{cases} \quad (1.1)$$

where \vec{n} is the unit normal vector of Γ and

$$\begin{aligned} \Gamma &:= \Gamma^x \cup \Gamma^y, & \Gamma^x &:= \cup_{p=1}^{m-1} \Gamma_p^x, & \Gamma^y &:= \cup_{q=1}^{m-1} \Gamma_q^y, \\ \Gamma_p^x &:= \left\{ (x, y) : x = \frac{p}{m}, y \in (0, 1), \text{ and } \text{mod}(ym, 1) \neq 0 \right\}, & 1 \leq p \leq m-1, \\ \Gamma_q^y &:= \left\{ (x, y) : y = \frac{q}{m}, x \in (0, 1), \text{ and } \text{mod}(xm, 1) \neq 0 \right\}, & 1 \leq q \leq m-1, \end{aligned} \quad (1.2)$$

where m is a positive integer. Note that

$$\Omega, \Gamma_p^x, \Gamma_q^y, \Gamma^x, \Gamma^y, \Gamma, \Omega \setminus \bar{\Gamma} \text{ are all open sets for every } 1 \leq p, q \leq m-1.$$

For $(\xi, y) \in \Gamma^x$ (i.e., on the vertical line of the cross-interface Γ),

$$[u](\xi, y) := \lim_{x \rightarrow \xi^+} u(x, y) - \lim_{x \rightarrow \xi^-} u(x, y), \quad [a \nabla u \cdot \vec{n}](\xi, y) := \lim_{x \rightarrow \xi^+} a(x, y) \frac{\partial u}{\partial x}(x, y) - \lim_{x \rightarrow \xi^-} a(x, y) \frac{\partial u}{\partial x}(x, y);$$

while for $(x, \zeta) \in \Gamma^y$ (i.e., on the horizontal line of the cross-interface Γ),

$$[u](x, \zeta) := \lim_{y \rightarrow \zeta^+} u(x, y) - \lim_{y \rightarrow \zeta^-} u(x, y), \quad [a \nabla u \cdot \vec{n}](x, \zeta) := \lim_{y \rightarrow \zeta^+} a(x, y) \frac{\partial u}{\partial y}(x, y) - \lim_{y \rightarrow \zeta^-} a(x, y) \frac{\partial u}{\partial y}(x, y).$$

We also define the subdomains of Ω as follows:

$$\Omega_{p,q} := \left\{ (x, y) : \frac{p-1}{m} < x < \frac{p}{m}, \frac{q-1}{m} < y < \frac{q}{m} \right\}, \quad 1 \leq p, q \leq m. \quad (1.3)$$

Clearly, a is a constant in each $\Omega_{p,q}$ and

$$\cup_{p=1}^m \cup_{q=1}^m \Omega_{p,q} = \Omega \setminus \bar{\Gamma}.$$

In this paper, we discuss the model problem (1.1) under the following assumptions:

- (A1) The coefficient function a is a positive piecewise constant function in $\Omega \setminus \Gamma$ (see Fig. 1 for an illustration).
- (A2) The source term f is continuous in Ω .

The rest of this paper is structured as follows:

In Section 2, we present second-order finite element and finite difference methods using uniform Cartesian grids. Precisely, we illustrate second-order finite element method in Section 2.1 and second-order finite difference method in Section 2.2.

In Section 3, we provide 7 numerical examples in the following two cases:

- We examine the model problem (1.1) using a high-contrast and low-frequency coefficient function in Example 1, and a low-contrast and relatively high-frequency coefficient function in Examples 2 and 3. Based on performances of the FEM and FDM solutions presented in Figs. 6 to 8, we observe that the FEM and FDM yield similar numerical solutions.
- We test the model problem (1.1) with high-contrast and relatively high-frequency coefficient functions in Examples 4 to 7. From performances of the FEM and FDM solutions in Figs. 9 to 12, we observe that FEM and FDM produce completely different numerical solutions.

$a = 10^{-3}$	$a = 10^3$	$a = 10^{-3}$	$a = 10^3$
$a = 10^3$	$a = 10^{-3}$	$a = 10^3$	$a = 10^{-3}$
$a = 10^{-3}$	$a = 10^3$	$a = 10^{-3}$	$a = 10^3$
$a = 10^3$	$a = 10^{-3}$	$a = 10^3$	$a = 10^{-3}$

$\Omega_{1,4}$	$\Omega_{2,4}$	$\Omega_{3,4}$	$\Omega_{4,4}$
$\Omega_{1,3}$	$\Omega_{2,3}$	$\Omega_{3,3}$	$\Omega_{4,3}$
$\Omega_{1,2}$	$\Omega_{2,2}$	$\Omega_{3,2}$	$\Omega_{4,2}$
$\Omega_{1,1}$	$\Omega_{2,1}$	$\Omega_{3,1}$	$\Omega_{4,1}$

FIGURE 1. An example for the coefficient function a (left) and subdomains $\Omega_{p,q}$ (right) for the model problem in (1.1) with $m = 4$.

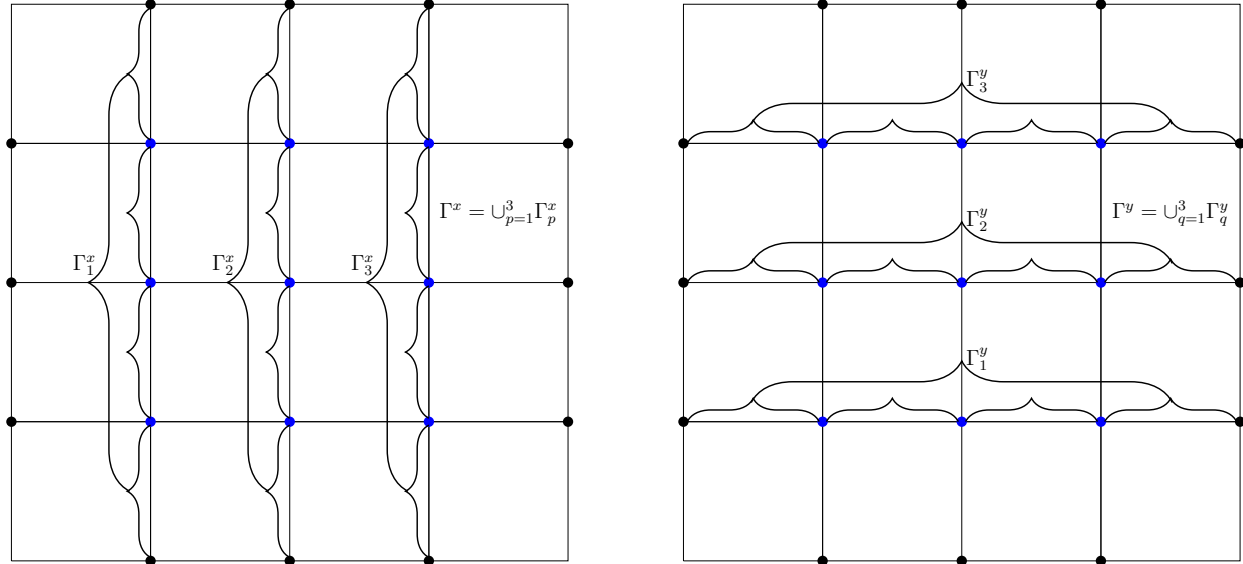


FIGURE 2. An illustration for the vertical lines Γ^x in (1.2) of the cross-interface Γ for the model problem (1.1) with $m = 4$ (left). An illustration for the horizontal lines Γ^y in (1.2) of the cross-interface Γ for the model problem (1.1) with $m = 4$ (right). Note that $\Gamma = \Gamma^x \cup \Gamma^y$, all Γ^x_p and Γ^y_q are open sets for $1 \leq p, q \leq 3$. The intersection points $\overline{\Gamma^x} \cap \overline{\Gamma^y}$ are indicated by the blue color and points on $\overline{\Gamma} \cap \partial\Omega$ are indicated by the black color.

In Section 4, we present several possible reasons to explain the above numerical results. In Section 5, we highlight the key contributions of this paper.

2. SECOND-ORDER FINITE ELEMENT AND FINITE DIFFERENCE METHODS USING UNIFORM CARTESIAN GRIDS

In this section, we present second-order finite element and finite difference methods on uniform Cartesian grids for the elliptic cross-interface problem in (1.1). We define that

$$x_i := ih, \quad i = 0, 1, \dots, N, \quad \text{and} \quad y_j := jh, \quad j = 0, 1, \dots, N, \quad (2.1)$$

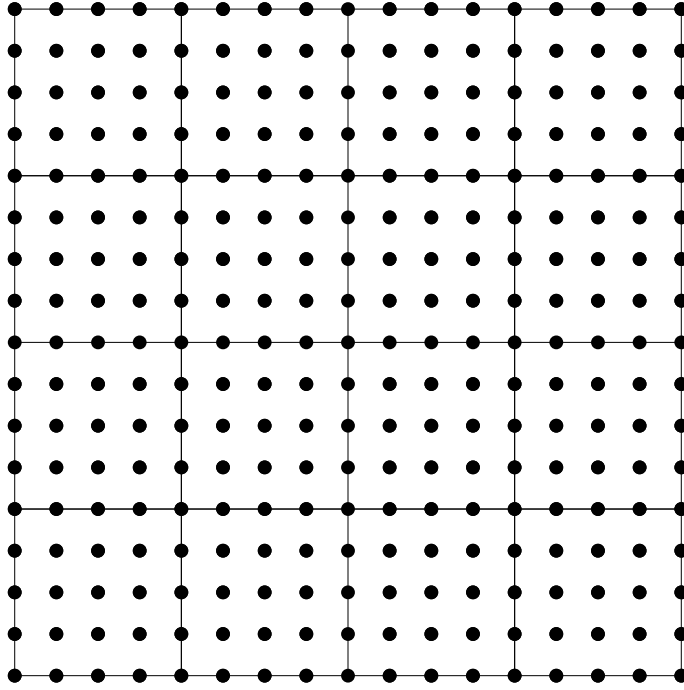


FIGURE 3. An example for uniform Cartesian grids of the problem (1.1)

where the uniform Cartesian mesh size $h := \frac{1}{N}$ is chosen for some positive integer N such that all intersection points $(x, y) \in \overline{\Gamma^x} \cap \overline{\Gamma^y}$ are grid points and some grid points lie on the vertical/horizontal interface lines (see Fig. 3 for an example with $m = 4$, $h = 1/16$ and $N = 16$).

2.1. Second-order finite element method. We use the standard second-order finite element method with piecewise linear basis and continuous functions to solve (1.1). Precisely, let's define the following 1D piecewise linear and continuous functions on $\{x_0, x_1, \dots, x_N\}$ and $\{y_0, y_1, \dots, y_N\}$ respectively:

$$\phi_i(x) := \begin{cases} \frac{x - x_{i-1}}{x_i - x_{i-1}} & \text{if } x_{i-1} \leq x \leq x_i, \\ \frac{x_{i+1} - x}{x_{i+1} - x_i} & \text{if } x_i \leq x \leq x_{i+1}, \\ 0 & \text{else,} \end{cases} \quad \phi_j(y) := \begin{cases} \frac{y - y_{j-1}}{y_j - y_{j-1}} & \text{if } y_{j-1} \leq y \leq y_j, \\ \frac{y_{j+1} - y}{y_{j+1} - y_j} & \text{if } y_j \leq y \leq y_{j+1}, \\ 0 & \text{else,} \end{cases}$$

where $1 \leq i, j \leq N - 1$. Then we define the 2D basis functions, and the continuous piecewise linear finite element space as follows:

$$\phi_{i,j} := \phi_i(x)\phi_j(y), \quad 1 \leq i, j \leq N - 1,$$

$$V_h := \{\phi_{i,j} : 1 \leq i, j \leq N - 1\}.$$

Let u_h^E be the numerical finite element method solution of the exact solution u of the elliptic cross-interface problem (1.1) using the mesh size $h = 1/N$. Then the standard finite element method implies

$$u_h^E := \sum_{i=1}^{N-1} \sum_{j=1}^{N-1} c_{i,j} \phi_{i,j},$$

where every $c_{i,j}$ is to-be-determined constant for $1 \leq i, j \leq N - 1$ by solving the following weak formulation of (1.1):

$$\int_{\Omega} a \nabla u_h^E \cdot \nabla v = \int_{\Omega} f v, \quad \text{for all } v \in V_h.$$

To verify the convergence rate of the finite element solution, we also define that

$$(u_h^E)_{i,j} = u_h^E(x_i, y_j), \quad \text{for } 1 \leq i, j \leq N-1, \quad (2.2)$$

where (x_i, y_j) is defined in (2.1).

2.2. Second-order finite difference method. We use the standard second-order 5-point finite difference method for the interior grid point $(x_i, y_j) \in \Omega \setminus \Gamma$ (see the first panel of Fig. 4). For the interface grid point $(x_i, y_j) \in \Gamma := \Gamma^x \cup \Gamma^y$ (see the second and third panels of Fig. 4), we use second-order 5-point finite difference methods based on second-order 3-point backward/forward upwind schemes.

Let $(u_h^D)_{i,j}$ be the value of the numerical finite difference method solution u_h^D of the exact solution u of the elliptic cross-interface problem (1.1), at the grid point (x_i, y_j) using the mesh size $h = 1/N$. For the sake of brevity, we also define that

$$u_{i,j} = u(x_i, y_j), \quad a_{i,j} = a(x_i, y_j), \quad f_{i,j} = f(x_i, y_j).$$

Then we use the well-known 5-point finite difference method at $(x_i, y_j) \in \Omega \setminus \Gamma$ in the following

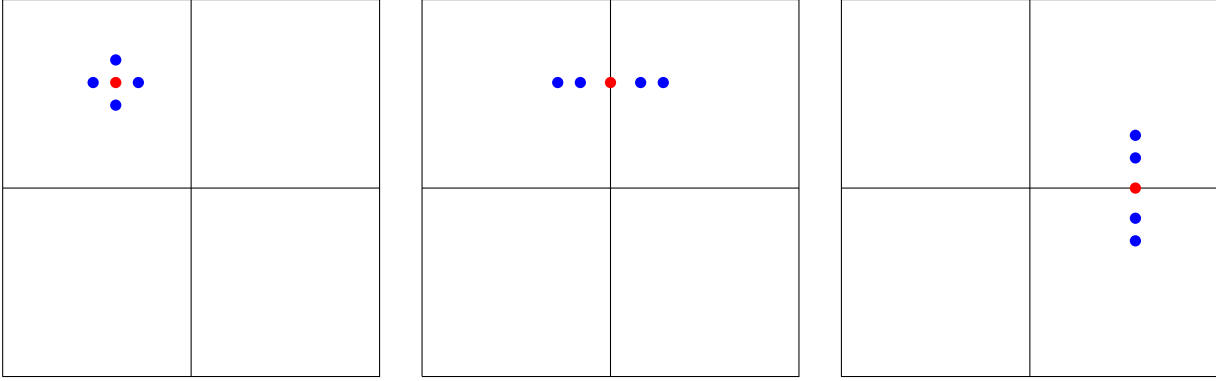


FIGURE 4. First panel: 5-point finite difference scheme in Theorem 2.1 with $(x_i, y_j) \in \Omega \setminus \Gamma$. Second panel: 5-point finite difference scheme in Theorem 2.2 with $(x_i, y_j) \in \Gamma^x$. Third panel: 5-point finite difference scheme in Theorem 2.3 with $(x_i, y_j) \in \Gamma^y$. The grid point (x_i, y_j) is marked in red.

theorem:

Theorem 2.1. Consider the interior grid point $(x_i, y_j) \in \Omega \setminus \Gamma$. Then the following 5-point finite difference scheme (see the first panel of Fig. 4)

$$a_{i,j} \left((u_h^D)_{i-1,j} + (u_h^D)_{i+1,j} + (u_h^D)_{i,j-1} + (u_h^D)_{i,j+1} - 4(u_h^D)_{i,j} \right) = -h^2 f_{i,j},$$

is the second-order consistent at the interior grid point $(x_i, y_j) \in \Omega \setminus \Gamma$.

For the interface grid point $(x_i, y_j) \in \Gamma^x$, we have that the second-order 3-point backward upwind scheme to approximate $u_x(x_i, y_j)$ is

$$\frac{\partial u}{\partial x}(x_i, y_j) = \frac{3u_{i,j} - 4u_{i-1,j} + u_{i-2,j}}{2h} + \mathcal{O}(h^2), \quad (2.3)$$

and the second-order 3-point forward upwind scheme to approximate $u_x(x_i, y_j)$ is

$$\frac{\partial u}{\partial x}(x_i, y_j) = \frac{-3u_{i,j} + 4u_{i+1,j} - u_{i+2,j}}{2h} + \mathcal{O}(h^2). \quad (2.4)$$

Since the coefficient function a is a piecewise constant function in $\Omega \setminus \Gamma$ (see Figs. 1 and 3 for illustrations), we have

$$\begin{aligned} [a\nabla u \cdot \vec{n}](x_i, y_j) &= a(x_i + h, y_j) \frac{-3u_{i,j} + 4u_{i+1,j} - u_{i+2,j}}{2h} \\ &\quad - a(x_i - h, y_j) \frac{3u_{i,j} - 4u_{i-1,j} + u_{i-2,j}}{2h} + \mathcal{O}(h^2), \end{aligned} \quad (2.5)$$

for $(x_i, y_j) \in \Gamma^x$. By $[a\nabla u \cdot \vec{n}] = 0$ on Γ^x , we obtain that

$$\frac{1}{2h} \left(a(x_i + h, y_j) (-3u_{i,j} + 4u_{i+1,j} - u_{i+2,j}) - a(x_i - h, y_j) (3u_{i,j} - 4u_{i-1,j} + u_{i-2,j}) \right) = 0,$$

has a second order of consistency at the interface grid point $(x_i, y_j) \in \Gamma^x$.

In summary, we have the second-order 5-point finite difference schemes at $(x_i, y_j) \in \Gamma := \Gamma^x \cup \Gamma^y$ in the following Theorems 2.2 and 2.3.

Theorem 2.2. *Consider the interface grid point $(x_i, y_j) \in \Gamma^x$. Let $a^- = a(x_i - h, y_j)$ and $a^+ = a(x_i + h, y_j)$. Then the following 5-point finite difference scheme (see the second panel of Fig. 4)*

$$-a^-(u_h^D)_{i-2,j} + 4a^-(u_h^D)_{i-1,j} - 3(a^- + a^+)(u_h^D)_{i,j} + 4a^+(u_h^D)_{i+1,j} - a^+(u_h^D)_{i+2,j} = 0,$$

has a second order of consistency at the interface grid point $(x_i, y_j) \in \Gamma^x$.

Theorem 2.3. *Consider the interface grid point $(x_i, y_j) \in \Gamma^y$. Let $a^- = a(x_i, y_j - h)$ and $a^+ = a(x_i, y_j + h)$. Then the following 5-point finite difference scheme (see the third panel of Fig. 4)*

$$-a^-(u_h^D)_{i,j-2} + 4a^-(u_h^D)_{i,j-1} - 3(a^- + a^+)(u_h^D)_{i,j} + 4a^+(u_h^D)_{i,j+1} - a^+(u_h^D)_{i,j+2} = 0,$$

has a second order of consistency at the interface grid point $(x_i, y_j) \in \Gamma^y$.

Remark 2.4. *The second-order 5-point schemes in Theorems 2.2 and 2.3 can also be derived from [15, (A.6)-(A.9)] by choosing $M = 2$ and applying two homogeneous jump conditions.*

By the definition of the uniform Cartesian grid in (2.1) of the model problem (1.1), we also need to provide the finite difference scheme at the intersection grid point $(x_i, y_j) \in \overline{\Gamma^x} \cap \overline{\Gamma^y}$ (see Fig. 3 for an illustration). But the schemes in Theorems 2.1 to 2.3 do not use any intersection grid points $(x_i, y_j) \in \overline{\Gamma^x} \cap \overline{\Gamma^y}$. So it is not necessary to propose the finite difference scheme at the grid point $\{(x_i, y_j) : (x_i, y_j) \in \overline{\Gamma^x} \cap \overline{\Gamma^y}\}$. I.e., we only compute

$$(u_h^D)_{i,j}, \quad 0 \leq i, j \leq N, \quad \text{and} \quad (x_i, y_j) \notin \overline{\Gamma^x} \cap \overline{\Gamma^y},$$

in the finite difference method (see Fig. 5 for an illustration).

3. NUMERICAL EXPERIMENTS

Recall that $(u_h^E)_{i,j}$ and $(u_h^D)_{i,j}$ are the finite element and finite difference solutions u_h^E and u_h^D respectively of the model problem (1.1) at (x_i, y_j) using the mesh size h , where

$$x_i := ih, \quad i = 0, 1, \dots, N, \quad \text{and} \quad y_j := jh, \quad j = 0, 1, \dots, N,$$

$h := 1/N$ for some integer N , and $\Omega := (0, 1)^2$.

We shall evaluate finite element and finite difference methods in the l_2 norm of the errors given by:

$$\|u_h^E - u_{h/2}^E\|_2 := h \sqrt{\sum_{i=0}^N \sum_{j=0}^N \left| (u_h^E)_{i,j} - (u_{h/2}^E)_{2i,2j} \right|^2},$$

and

$$\|u_h^D - u_{h/2}^D\|_2 := h \sqrt{\sum_{\substack{i=0 \\ (x_i, y_j) \notin \overline{\Gamma^x} \cap \overline{\Gamma^y}}}^N \sum_{j=0}^N \left| (u_h^D)_{i,j} - (u_{h/2}^D)_{2i,2j} \right|^2}.$$

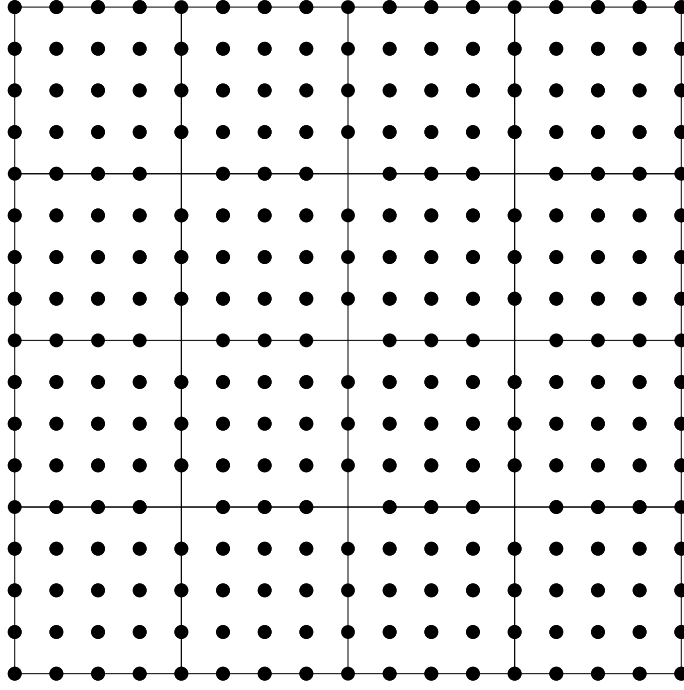


FIGURE 5. The computed numerical solutions $(u_h^D)_{i,j}$ with $0 \leq i, j \leq N$, and $(x_i, y_j) \notin \overline{\Gamma^x} \cap \overline{\Gamma^y}$ in the finite difference method.

Furthermore, we also provide results for the infinity norm of the errors given by:

$$\|u_h^E - u_{h/2}^E\|_\infty := \max_{0 \leq i \leq N, 0 \leq j \leq N} |(u_h^E)_{i,j} - (u_{h/2}^E)_{2i,2j}|,$$

and

$$\|u_h^D - u_{h/2}^D\|_\infty := \max_{\substack{0 \leq i \leq N, 0 \leq j \leq N \\ (x_i, y_j) \notin \overline{\Gamma^x} \cap \overline{\Gamma^y}}} |(u_h^D)_{i,j} - (u_{h/2}^D)_{2i,2j}|.$$

Example 1. Let $f = 1$ and $m = 2$ in (1.1). The coefficient function a in (1.1) is given in the first row of Fig. 6. Note that $a = 1000$ in yellow squares and $a = 0.001$ in blue squares. The numerical results are displayed in Table 1 and Fig. 6.

TABLE 1. Performance in Example 1 of finite element and finite difference methods on uniform Cartesian meshes.

h	Use FEM in Section 2.1				Use FDM in Section 2.2			
	$\ u_h^E - u_{h/2}^E\ _2$	order	$\ u_h^E - u_{h/2}^E\ _\infty$	order	$\ u_h^D - u_{h/2}^D\ _2$	order	$\ u_h^D - u_{h/2}^D\ _\infty$	order
$\frac{1}{2^2}$	1.4205E+00		4.0179E+00		6.9053E-01		1.9531E+00	
$\frac{1}{2^3}$	3.1139E-01	2.19	7.7007E-01	2.38	2.5329E-01	1.45	6.1753E-01	1.66
$\frac{1}{2^4}$	7.3853E-02	2.08	1.7475E-01	2.14	6.9442E-02	1.87	1.6578E-01	1.90
$\frac{1}{2^5}$	1.8132E-02	2.03	4.2797E-02	2.03	1.7806E-02	1.96	4.2243E-02	1.97
$\frac{1}{2^6}$	4.5073E-03	2.01	1.0647E-02	2.01	4.4838E-03	1.99	1.0612E-02	1.99

Example 2. Let $f = 1$ and $m = 4$ in (1.1). The coefficient function a in (1.1) is given in the first row of Fig. 7. Note that $a = 10$ in yellow squares and $a = 1$ in blue squares. The numerical results are displayed in Table 2 and Fig. 7.

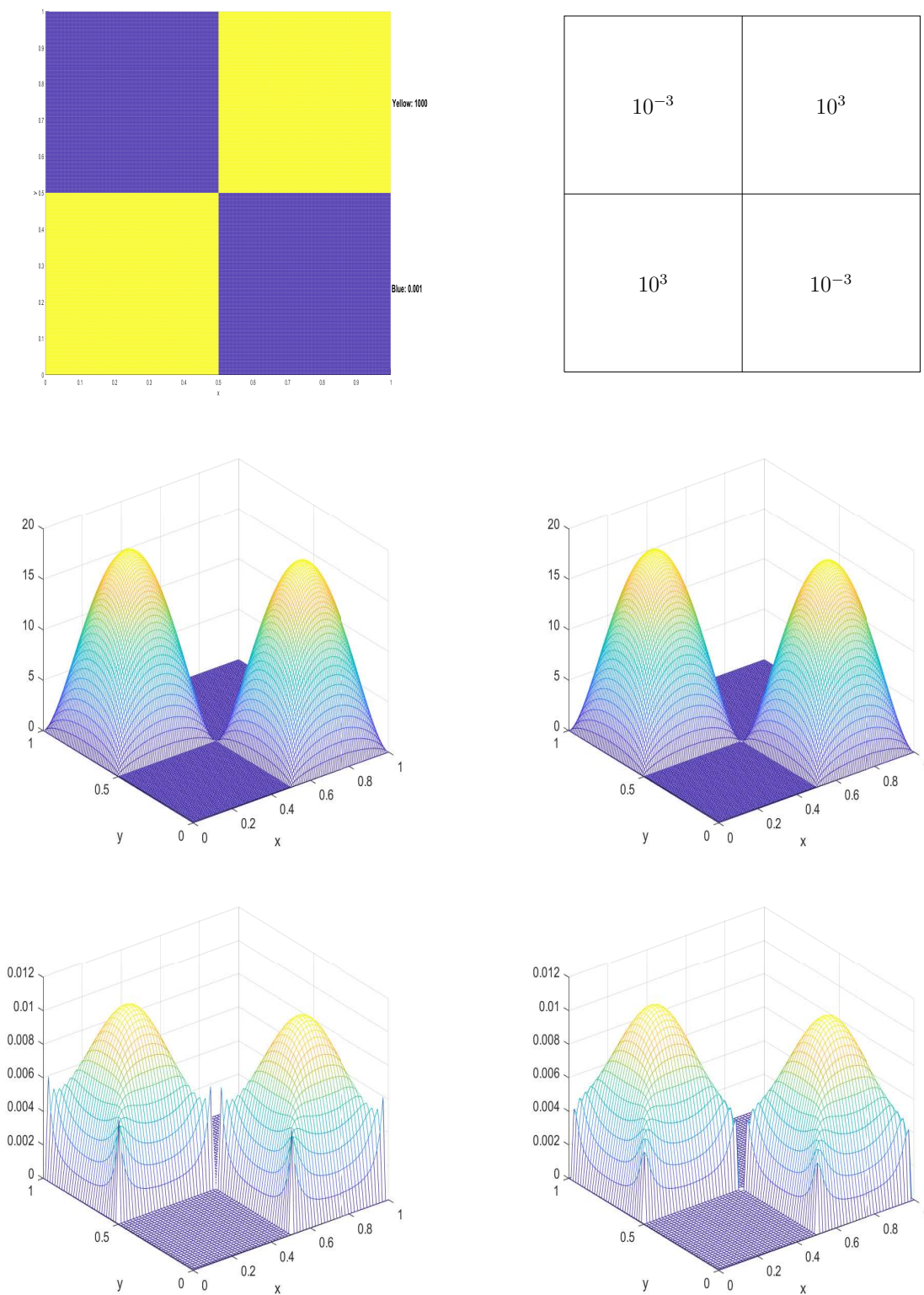


FIGURE 6. Example 1: The first row: the coefficient function a with $a = 1000$ in yellow squares, $a = 0.001$ in blue squares, and $m = 2$. The second row: the finite element solution $(u_h^E)_{i,j}$ (left) and the finite difference solution $(u_h^D)_{i,j}$ (right) at all (x_i, y_j) with $h = 1/2^7$. The third row: $|(u_h^E)_{i,j} - (u_{h/2}^E)_{2i,2j}|$ (left) and $|(u_h^D)_{i,j} - (u_{h/2}^D)_{2i,2j}|$ (right) at all (x_i, y_j) with $h = 1/2^6$.

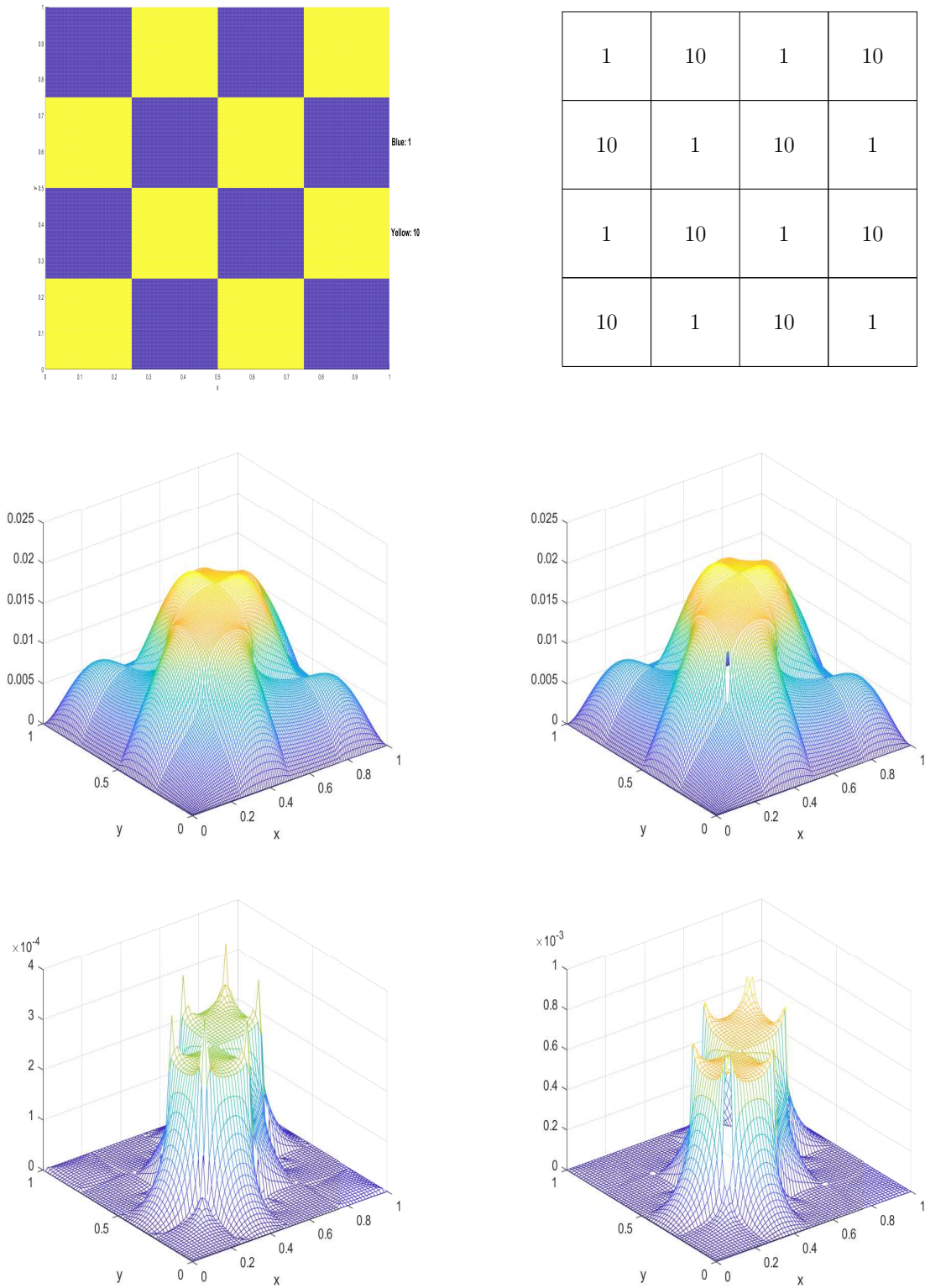


FIGURE 7. Example 2: The first row: the coefficient function a with $a = 10$ in yellow squares, $a = 1$ in blue squares, and $m = 4$. The second row: the finite element solution $(u_h^E)_{i,j}$ (left) and the finite difference solution $(u_h^D)_{i,j}$ (right) at all (x_i, y_j) with $h = 1/2^7$. The third row: $|(u_h^E)_{i,j} - (u_{h/2}^E)_{2i,2j}|$ (left) and $|(u_h^D)_{i,j} - (u_{h/2}^D)_{2i,2j}|$ (right) at all (x_i, y_j) with $h = 1/2^6$.

TABLE 2. Performance in Example 2 of finite element and finite difference methods on uniform Cartesian meshes.

h	Use FEM in Section 2.1				Use FDM in Section 2.2			
	$\ u_h^E - u_{h/2}^E\ _2$	order	$\ u_h^E - u_{h/2}^E\ _\infty$	order	$\ u_h^D - u_{h/2}^D\ _2$	order	$\ u_h^D - u_{h/2}^D\ _\infty$	order
$\frac{1}{2^3}$	5.0839E-04		1.5140E-03		1.9897E-03		4.9999E-03	
$\frac{1}{2^4}$	3.1692E-04	0.68	8.6841E-04	0.80	1.0171E-03	0.97	2.4015E-03	1.06
$\frac{1}{2^5}$	2.0231E-04	0.65	5.8430E-04	0.57	5.4431E-04	0.90	1.3437E-03	0.84
$\frac{1}{2^6}$	1.2417E-04	0.70	3.9910E-04	0.55	3.0031E-04	0.86	8.2004E-04	0.71

Example 3. Let $f = 1$ and $m = 8$ in (1.1). The coefficient function a in (1.1) is given in the first row of Fig. 8. Note that $a = 10$ in yellow squares and $a = 1$ in blue squares. The numerical results are displayed in Table 3 and Fig. 8.

TABLE 3. Performance in Example 3 of finite element and finite difference methods on uniform Cartesian meshes.

h	Use FEM in Section 2.1				Use FDM in Section 2.2			
	$\ u_h^E - u_{h/2}^E\ _2$	order	$\ u_h^E - u_{h/2}^E\ _\infty$	order	$\ u_h^D - u_{h/2}^D\ _2$	order	$\ u_h^D - u_{h/2}^D\ _\infty$	order
$\frac{1}{2^4}$	8.0188E-04		1.7532E-03		2.8484E-03		6.7857E-03	
$\frac{1}{2^5}$	4.9292E-04	0.70	1.0323E-03	0.76	1.4258E-03	1.00	2.9368E-03	1.21
$\frac{1}{2^6}$	3.0106E-04	0.71	6.3921E-04	0.69	7.7563E-04	0.88	1.5856E-03	0.89
$\frac{1}{2^7}$	1.8072E-04	0.74	3.9633E-04	0.69	4.2936E-04	0.85	8.9909E-04	0.82

Example 4. Let $f = 1$ and $m = 4$ in (1.1). The coefficient function a in (1.1) is given in the first row of Fig. 9. Note that $a = 1000$ in yellow squares and $a = 0.001$ in blue squares. The numerical results are displayed in Table 4 and Fig. 9.

TABLE 4. Performance in Example 4 of finite element and finite difference methods on uniform Cartesian meshes.

h	Use FEM in Section 2.1				Use FDM in Section 2.2			
	$\ u_h^E - u_{h/2}^E\ _2$	order	$\ u_h^E - u_{h/2}^E\ _\infty$	order	$\ u_h^D - u_{h/2}^D\ _2$	order	$\ u_h^D - u_{h/2}^D\ _\infty$	order
$\frac{1}{2^3}$	3.5513E-01		1.0045E+00		2.5237E+00		6.2348E+00	
$\frac{1}{2^4}$	7.7843E-02	2.19	1.9252E-01	2.38	1.5017E+00	0.75	3.4263E+00	0.86
$\frac{1}{2^5}$	1.8458E-02	2.08	4.3687E-02	2.14	9.5379E-01	0.65	2.1370E+00	0.68
$\frac{1}{2^6}$	4.5272E-03	2.03	1.0699E-02	2.03	6.5185E-01	0.55	1.4513E+00	0.56

Example 5. Let $f = 1$ and $m = 8$ in (1.1). The coefficient function a in (1.1) is given in the first row of Fig. 10. Note that $a = 1000$ in yellow squares and $a = 0.001$ in blue squares. The numerical results are displayed in Table 5 and Fig. 10.

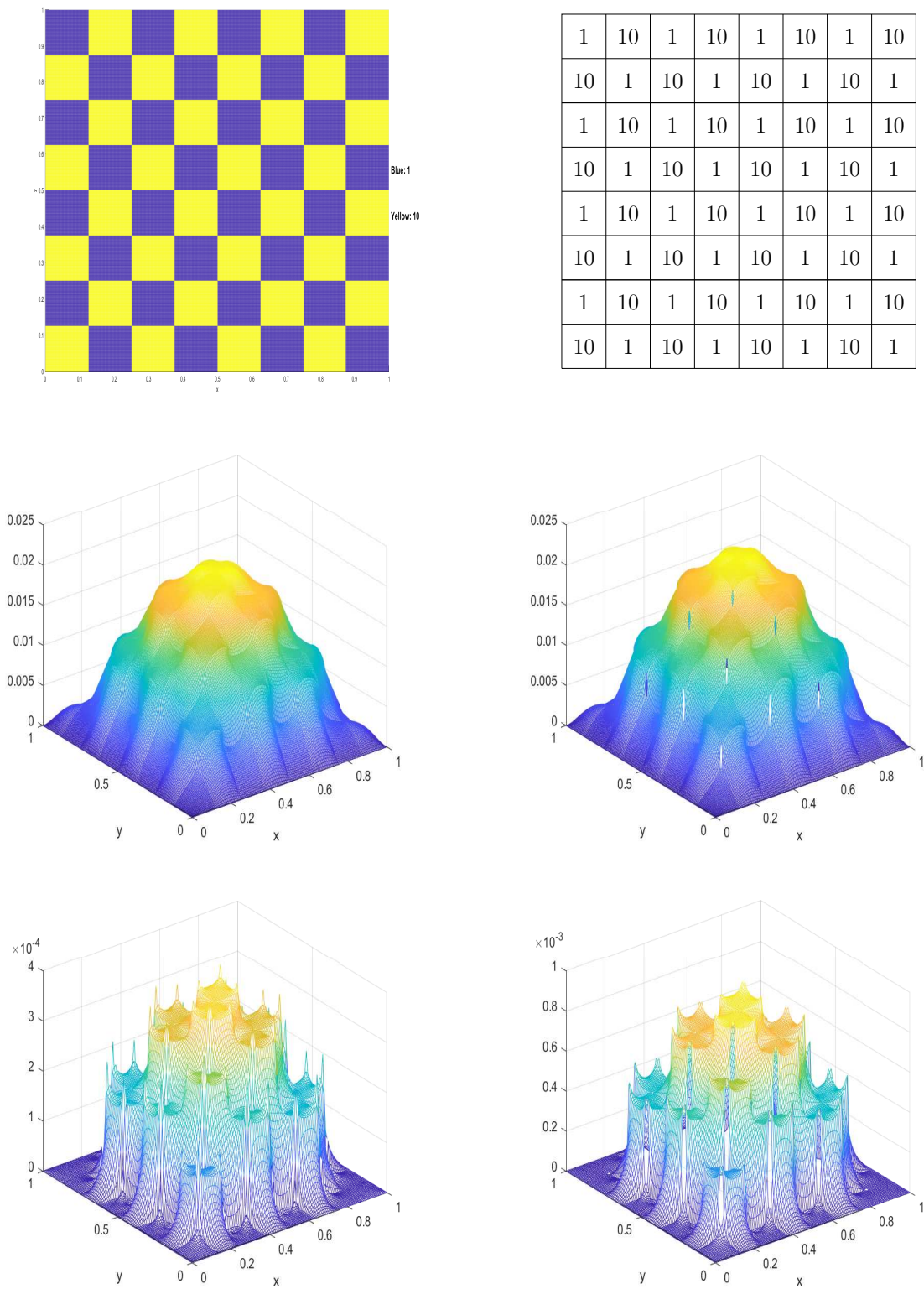


FIGURE 8. Example 3: The first row: the coefficient function a with $a = 10$ in yellow squares, $a = 1$ in blue squares, and $m = 8$. The second row: the finite element solution $(u_h^E)_{i,j}$ (left) and the finite difference solution $(u_h^D)_{i,j}$ (right) at all (x_i, y_j) with $h = 1/2^8$. The third row: $|(u_h^E)_{i,j} - (u_{h/2}^E)_{2i,2j}|$ (left) and $|(u_h^D)_{i,j} - (u_{h/2}^D)_{2i,2j}|$ (right) at all (x_i, y_j) with $h = 1/2^7$.

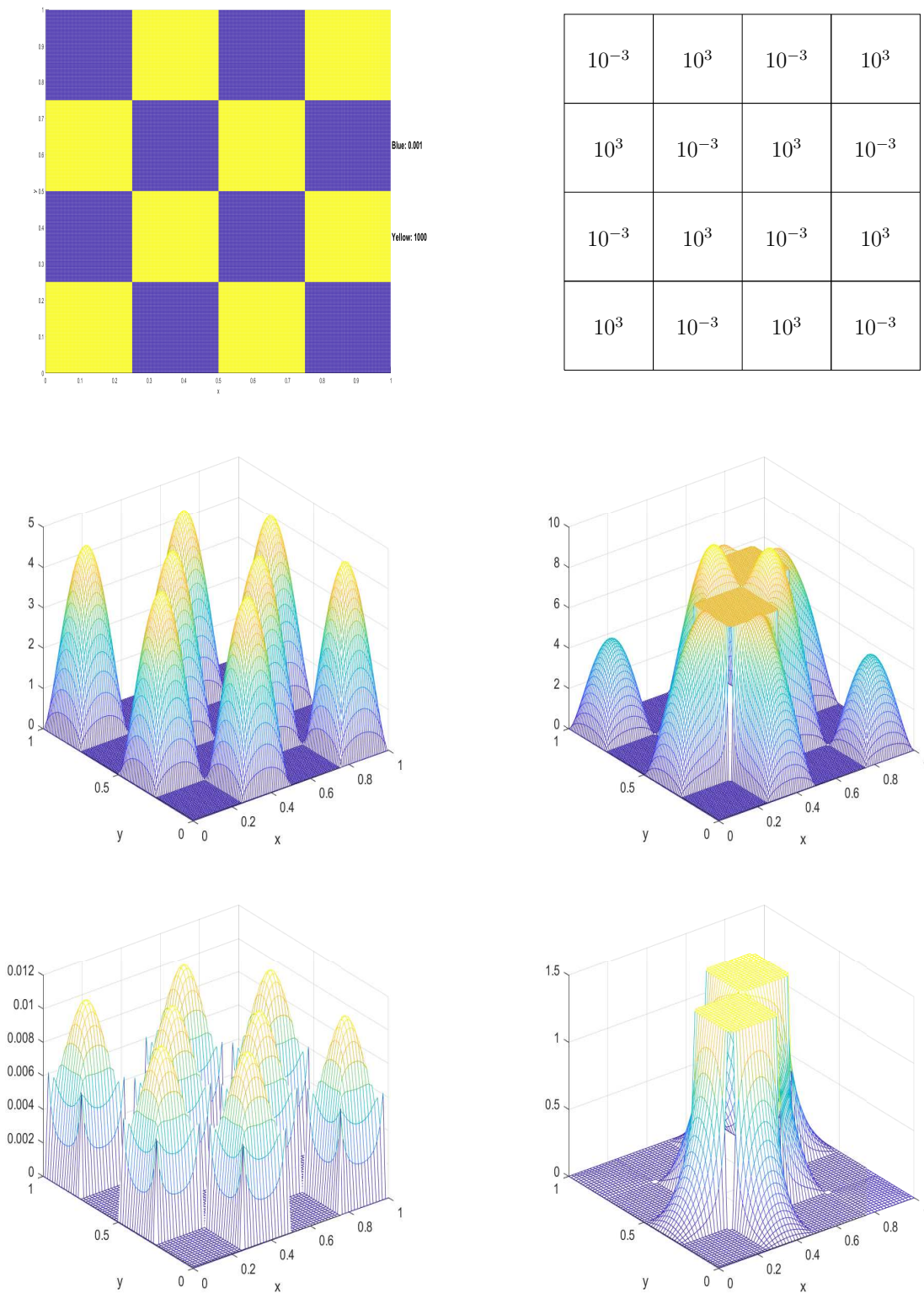


FIGURE 9. Example 4: The first row: the coefficient function a with $a = 1000$ in yellow squares, $a = 0.001$ in blue squares, and $m = 4$. The second row: the finite element solution $(u_h^E)_{i,j}$ (left) and the finite difference solution $(u_h^D)_{i,j}$ (right) at all (x_i, y_j) with $h = 1/2^7$. The third row: $|(u_h^E)_{i,j} - (u_{h/2}^E)_{2i,2j}|$ (left) and $|(u_h^D)_{i,j} - (u_{h/2}^D)_{2i,2j}|$ (right) at all (x_i, y_j) with $h = 1/2^6$.

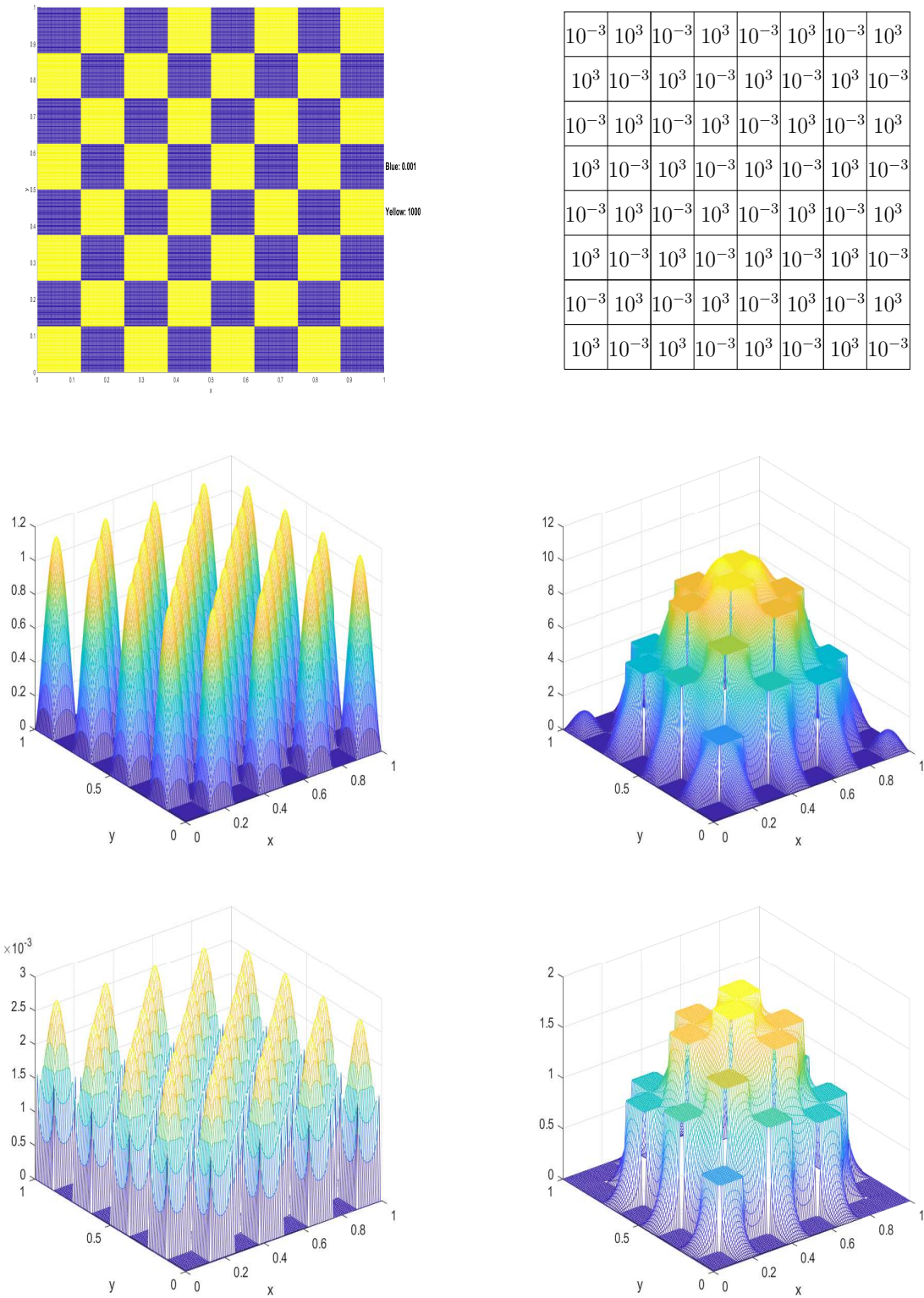


FIGURE 10. Example 5: The first row: the coefficient function a with $a = 1000$ in yellow squares, $a = 0.001$ in blue squares, and $m = 8$. The second row: the finite element solution $(u_h^E)_{i,j}$ (left) and the finite difference solution $(u_h^D)_{i,j}$ (right) at all (x_i, y_j) with $h = 1/2^8$. The third row: $|(u_h^E)_{i,j} - (u_{h/2}^E)_{2i,2j}|$ (left) and $|(u_h^D)_{i,j} - (u_{h/2}^D)_{2i,2j}|$ (right) at all (x_i, y_j) with $h = 1/2^7$.

TABLE 5. Performance in Example 5 of finite element and finite difference methods on uniform Cartesian meshes.

h	Use FEM in Section 2.1				Use FDM in Section 2.2			
	$\ u_h^E - u_{h/2}^E\ _2$	order	$\ u_h^E - u_{h/2}^E\ _\infty$	order	$\ u_h^D - u_{h/2}^D\ _2$	order	$\ u_h^D - u_{h/2}^D\ _\infty$	order
$\frac{1}{2^4}$	8.8776E-02		2.5112E-01		3.8360E+00		9.1066E+00	
$\frac{1}{2^5}$	1.9452E-02	2.19	4.8129E-02	2.38	2.1341E+00	0.85	4.3654E+00	1.06
$\frac{1}{2^6}$	4.6051E-03	2.08	1.0922E-02	2.14	1.3691E+00	0.64	2.7437E+00	0.67
$\frac{1}{2^7}$	1.1223E-03	2.04	2.6748E-03	2.03	9.4162E-01	0.54	1.8822E+00	0.54

Example 6. Let $f = 1$ and $m = 16$ in (1.1). The coefficient function a in (1.1) is given in the first row of Fig. 11. Note that $a = 1000$ in yellow squares and $a = 0.001$ in blue squares. The numerical results are displayed in Table 6 and Fig. 11.

TABLE 6. Performance in Example 6 of finite element and finite difference methods on uniform Cartesian meshes.

h	Use FEM in Section 2.1				Use FDM in Section 2.2			
	$\ u_h^E - u_{h/2}^E\ _2$	order	$\ u_h^E - u_{h/2}^E\ _\infty$	order	$\ u_h^D - u_{h/2}^D\ _2$	order	$\ u_h^D - u_{h/2}^D\ _\infty$	order
$\frac{1}{2^5}$	2.2187E-02		6.2779E-02		4.7871E+00		1.0605E+01	
$\frac{1}{2^6}$	4.8528E-03	2.19	1.2032E-02	2.38	2.5505E+00	0.91	4.9618E+00	1.10
$\frac{1}{2^7}$	1.1399E-03	2.09	2.7305E-03	2.14	1.6425E+00	0.63	3.1229E+00	0.67
$\frac{1}{2^8}$	2.6975E-04	2.08	6.6872E-04	2.03	1.1339E+00	0.53	2.1465E+00	0.54

Example 7. Let $f = 1$ and $m = 4$ in (1.1). The coefficient function a in (1.1) is given in the first row of Fig. 12. The numerical results are displayed in Table 7 and Fig. 12.

TABLE 7. Performance in Example 7 of finite element and finite difference methods on uniform Cartesian meshes.

h	Use FEM in Section 2.1				Use FDM in Section 2.2			
	$\ u_h^E - u_{h/2}^E\ _2$	order	$\ u_h^E - u_{h/2}^E\ _\infty$	order	$\ u_h^D - u_{h/2}^D\ _2$	order	$\ u_h^D - u_{h/2}^D\ _\infty$	order
$\frac{1}{2^3}$	5.7156E-04		2.8756E-03		3.9260E-03		1.1793E-02	
$\frac{1}{2^4}$	2.5777E-04	1.15	1.3236E-03	1.12	2.2782E-03	0.79	6.7839E-03	0.80
$\frac{1}{2^5}$	2.1484E-04	0.26	1.0128E-03	0.39	1.4528E-03	0.65	4.3152E-03	0.65
$\frac{1}{2^6}$	1.9528E-04	0.14	8.2897E-04	0.29	9.9857E-04	0.54	2.9800E-03	0.53

4. POSSIBLE EXPLANATIONS

The reason why the finite element method and finite difference method generate two distinct numerical solutions might be due to the severe singularities caused by high jumps in the coefficient

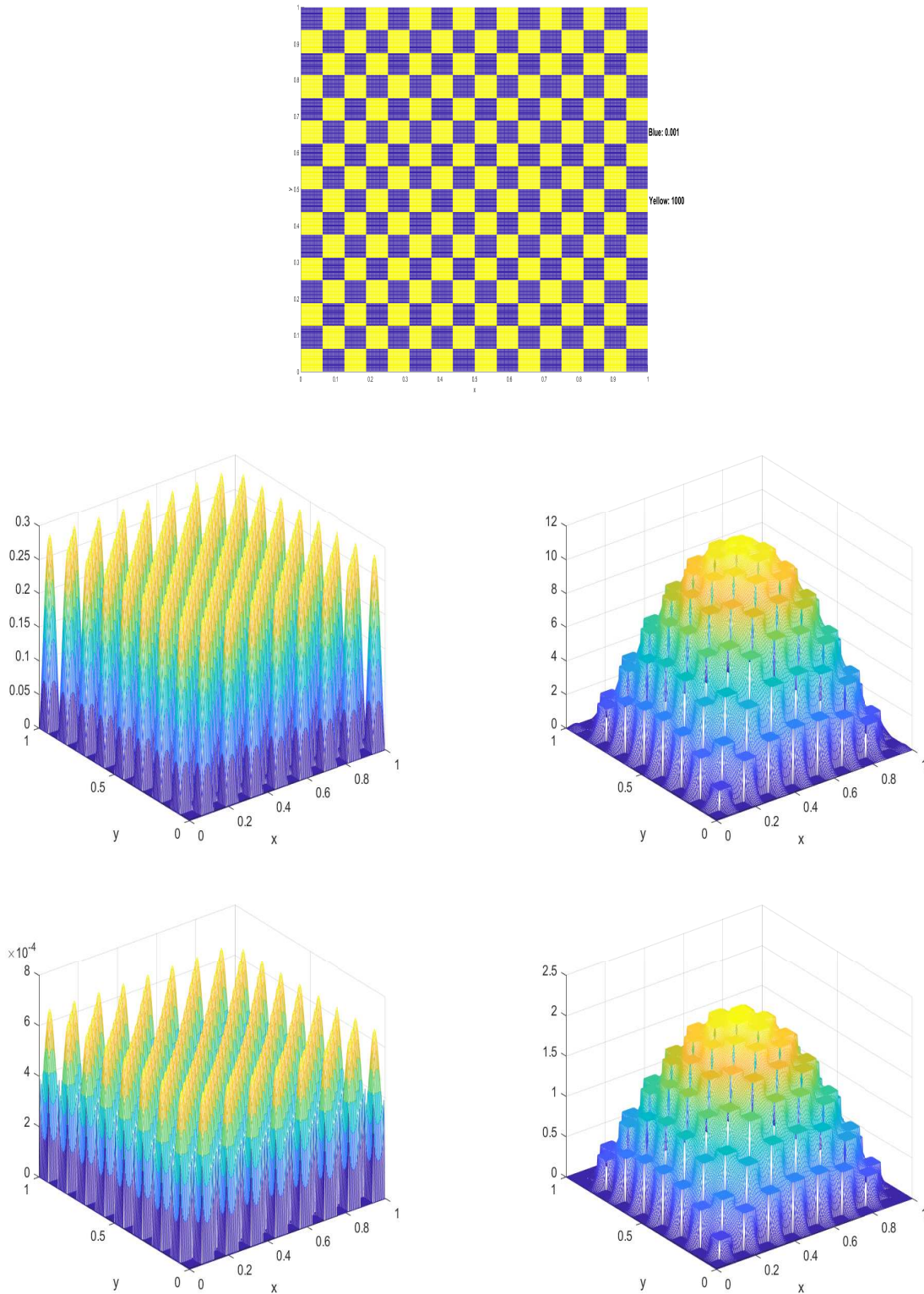
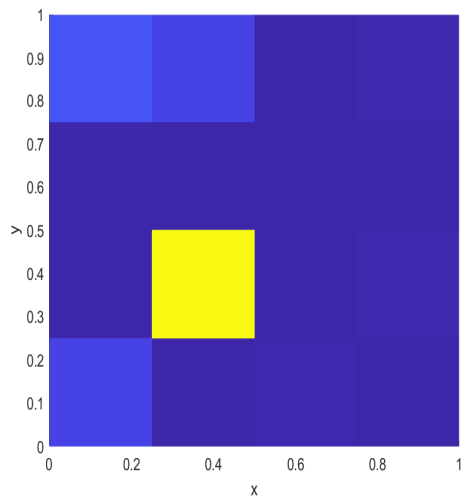


FIGURE 11. Example 6: The first row: the coefficient function a with $a = 1000$ in yellow squares, $a = 0.001$ in blue squares, and $m = 16$. The second row: the finite element solution $(u_h^E)_{i,j}$ (left) and the finite difference solution $(u_h^D)_{i,j}$ (right) at all (x_i, y_j) with $h = 1/2^8$. The third row: $|(u_h^E)_{i,j} - (u_{h/2}^E)_{2i,2j}|$ (left) and $|(u_h^D)_{i,j} - (u_{h/2}^D)_{2i,2j}|$ (right) at all (x_i, y_j) with $h = 1/2^8$.



150	100	1	10
5	0.45	0.5	1
0.4	1000	0.35	10
100	0.5	10	1

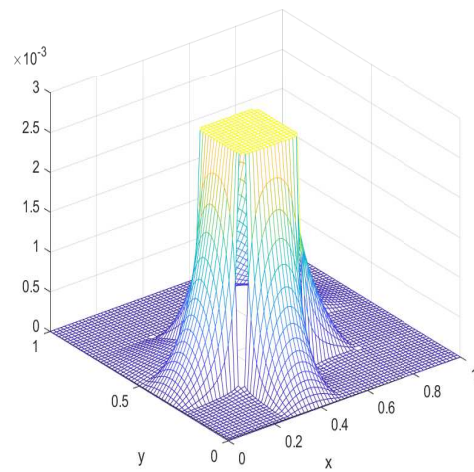
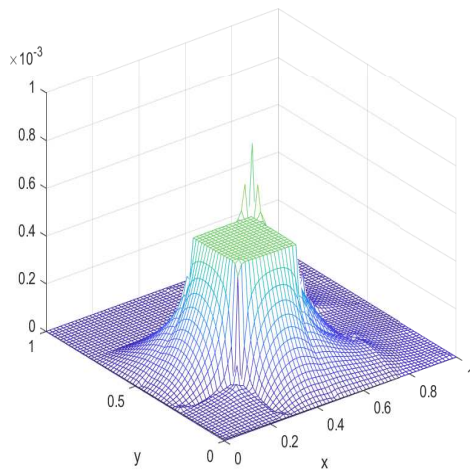
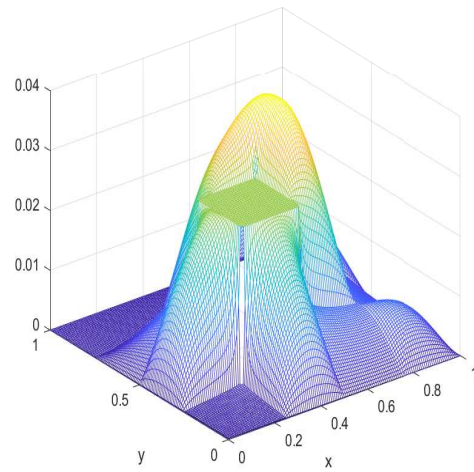
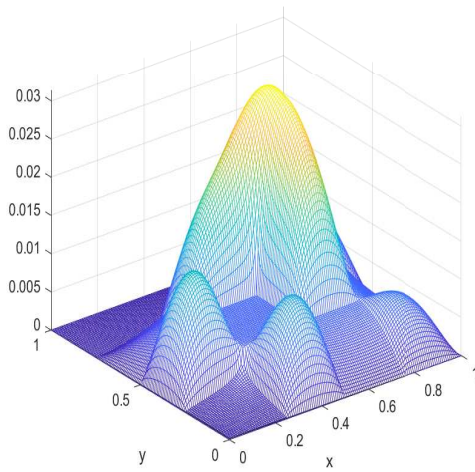


FIGURE 12. Example 7: The first row: the coefficient function a with $m = 4$. The second row: the finite element solution $(u_h^E)_{i,j}$ (left) and the finite difference solution $(u_h^D)_{i,j}$ (right) at all (x_i, y_j) with $h = 1/2^7$. The third row: $|(u_h^E)_{i,j} - (u_{h/2}^E)_{2i,2j}|$ (left) and $|(u_h^D)_{i,j} - (u_{h/2}^D)_{2i,2j}|$ (right) at all (x_i, y_j) with $h = 1/2^6$.

functions at the intersection points (see e.g. [5, 7, 18, 26–30, 38, 39, 41, 42]). Recall that $\cup_{p=1}^m \cup_{q=1}^m \Omega_{p,q} = \Omega \setminus \Gamma$ and a is a constant in each $\Omega_{p,q}$. Using [43, Assumption 4.43], we define that $P_\Omega := \{\Omega_{p,q}\}_{1 \leq p,q \leq m}$, i.e., P_Ω is the partition of Ω . By the discussions in [5, 7, 18, 26–30, 38, 39, 41, 42], we have that the exact solution u of the model problem (1.1) may satisfy $u \in H^{1+\lambda}(P_\Omega)$ with $0 < \lambda < 1$. For example: Let $\Omega = (-1, 1)^2$, $0 < \lambda < 1$, $\theta = \arctan\left(\frac{y}{x}\right)$,

$$a = \begin{cases} k^{-1} & 0 < \theta < \pi/2, \\ k & \pi/2 < \theta < \pi, \\ k^{-1} & \pi < \theta < 3\pi/2, \\ k & 3\pi/2 < \theta < 2\pi, \end{cases} \quad k = \tan(\lambda\pi/4), \quad (4.1)$$

$$\Gamma := \left\{ (x, y) : x = 0, y \in (-1, 0) \cup (0, 1) \right\} \cup \left\{ (x, y) : y = 0, x \in (-1, 0) \cup (0, 1) \right\},$$

and consider the following problem with a zero source term and the non-homogeneous Dirichlet boundary condition:

$$\begin{cases} -\nabla \cdot (a \nabla u) & = 0 & \text{in } \Omega \setminus \Gamma, \\ [u] & = 0 & \text{on } \Gamma, \\ [a \nabla u \cdot \vec{n}] & = 0 & \text{on } \Gamma, \\ u & = g & \text{on } \partial\Omega. \end{cases} \quad (4.2)$$

By [8, 28, 42], the analytical solution u of (4.2) is (see Fig. 13 for an illustration)

$$u = \begin{cases} u_1 = (\sqrt{x^2 + y^2})^\lambda \sin(\lambda\pi/4) \cos\left(\frac{\lambda(\pi-4\theta)}{4}\right) & 0 \leq \theta \leq \pi/2, \\ u_2 = (\sqrt{x^2 + y^2})^\lambda \cos(\lambda\pi/4) \sin\left(\frac{\lambda(3\pi-4\theta)}{4}\right) & \pi/2 \leq \theta \leq \pi, \\ u_3 = -(\sqrt{x^2 + y^2})^\lambda \sin(\lambda\pi/4) \cos\left(\frac{\lambda(5\pi-4\theta)}{4}\right) & \pi \leq \theta \leq 3\pi/2, \\ u_4 = -(\sqrt{x^2 + y^2})^\lambda \cos(\lambda\pi/4) \sin\left(\frac{\lambda(7\pi-4\theta)}{4}\right) & 3\pi/2 \leq \theta \leq 2\pi, \end{cases} \quad (4.3)$$

where the boundary function g in (4.2) can be obtained by plugging u in (4.3) into (4.2). Let $r = \sqrt{x^2 + y^2}$. Then

$$u_x = \begin{cases} (u_1)_x = \lambda r^{\lambda-1/2} \sin(\lambda\pi/4) \left\{ \cos\left(\frac{\lambda(\pi-4\theta)}{4}\right) x - \sin\left(\frac{\lambda(\pi-4\theta)}{4}\right) y \right\} & 0 < \theta < \pi/2, \\ (u_2)_x = \lambda r^{\lambda-1/2} \cos(\lambda\pi/4) \left\{ \sin\left(\frac{\lambda(3\pi-4\theta)}{4}\right) x + \cos\left(\frac{\lambda(3\pi-4\theta)}{4}\right) y \right\} & \pi/2 < \theta < \pi, \\ (u_3)_x = -\lambda r^{\lambda-1/2} \sin(\lambda\pi/4) \left\{ \cos\left(\frac{\lambda(5\pi-4\theta)}{4}\right) x - \sin\left(\frac{\lambda(5\pi-4\theta)}{4}\right) y \right\} & \pi < \theta < 3\pi/2, \\ (u_4)_x = -\lambda r^{\lambda-1/2} \cos(\lambda\pi/4) \left\{ \sin\left(\frac{\lambda(7\pi-4\theta)}{4}\right) x + \cos\left(\frac{\lambda(7\pi-4\theta)}{4}\right) y \right\} & 3\pi/2 < \theta < 2\pi, \end{cases} \quad (4.4)$$

$$u_y = \begin{cases} (u_1)_y = \lambda r^{\lambda-1/2} \sin(\lambda\pi/4) \left\{ \sin\left(\frac{\lambda(\pi-4\theta)}{4}\right) x + \cos\left(\frac{\lambda(\pi-4\theta)}{4}\right) y \right\} & 0 < \theta < \pi/2, \\ (u_2)_y = \lambda r^{\lambda-1/2} \cos(\lambda\pi/4) \left\{ -\cos\left(\frac{\lambda(3\pi-4\theta)}{4}\right) x + \sin\left(\frac{\lambda(3\pi-4\theta)}{4}\right) y \right\} & \pi/2 < \theta < \pi, \\ (u_3)_y = -\lambda r^{\lambda-1/2} \sin(\lambda\pi/4) \left\{ \sin\left(\frac{\lambda(5\pi-4\theta)}{4}\right) x + \cos\left(\frac{\lambda(5\pi-4\theta)}{4}\right) y \right\} & \pi < \theta < 3\pi/2, \\ (u_4)_y = -\lambda r^{\lambda-1/2} \cos(\lambda\pi/4) \left\{ -\cos\left(\frac{\lambda(7\pi-4\theta)}{4}\right) x + \sin\left(\frac{\lambda(7\pi-4\theta)}{4}\right) y \right\} & 3\pi/2 < \theta < 2\pi. \end{cases} \quad (4.5)$$

Choose

$$\lambda = \arctan\left(10^{-3}\right) \frac{4}{\pi} \approx 0.001273239120322. \quad (4.6)$$

We have that $k = 10^{-3}$ in (4.1), and the u_x in (4.4) and u_y in (4.5) meet that

$$\left| \frac{\partial u_i(0,0)}{\partial x} \right| = \infty, \quad \left| \frac{\partial u_i(0,0)}{\partial y} \right| = \infty, \quad \text{for } i = 1, 2, 3, 4.$$

Note that a in (4.1) and u in (4.3) with (4.6) are shown in Fig. 13.

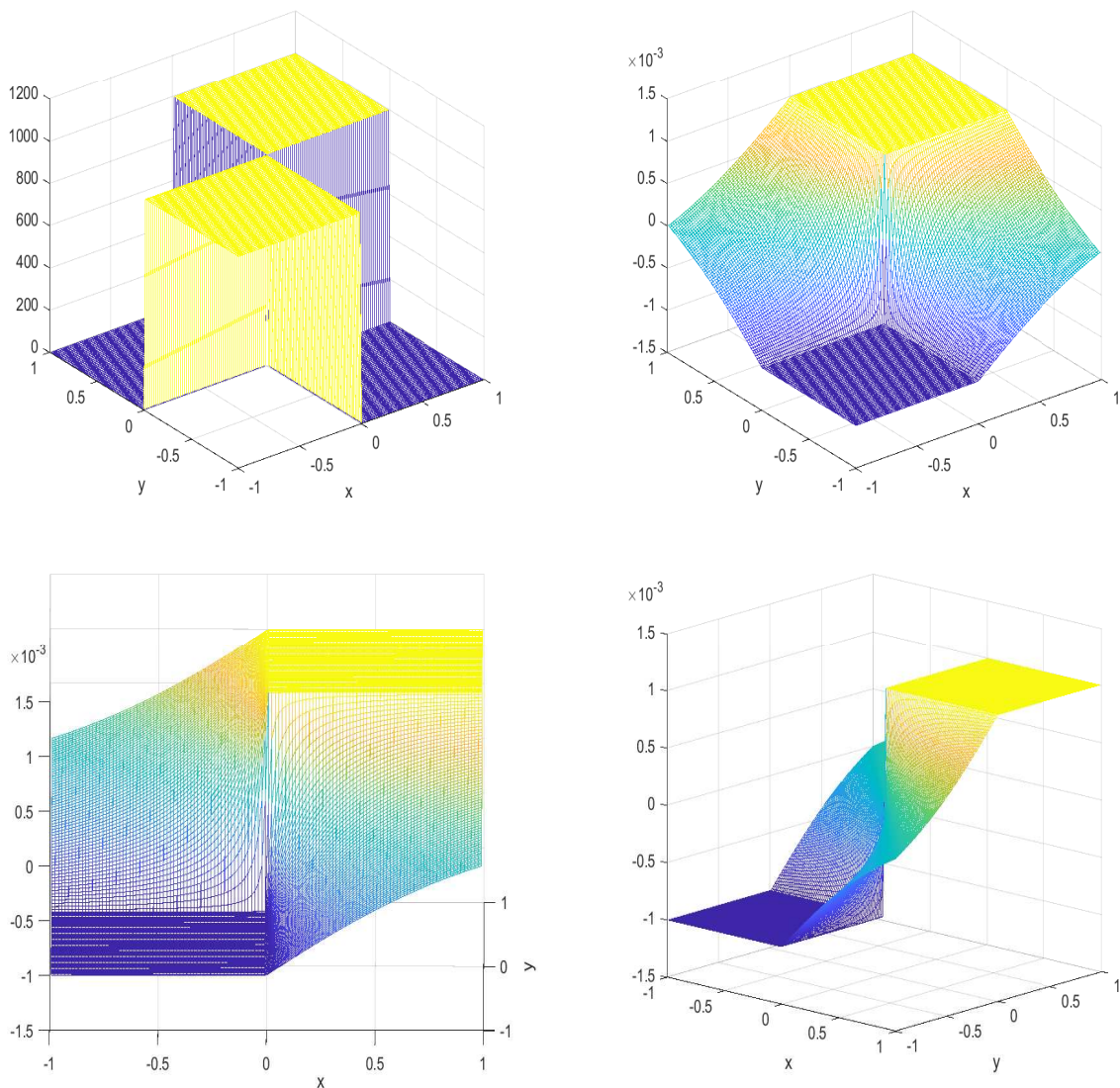


FIGURE 13. The first row: the coefficient function a with $a = 1000$ in yellow squares, $a = 0.001$ in blue squares (left) and the analytical solution u in (4.3) with λ in (4.6) (right). The second row: the analytical solution u in (4.3) with λ in (4.6).

For the model problem (1.1), [43, Section 4.5] discussed the error analysis and convergence proof of the discontinuous Galerkin method. Specifically, by adding the penalty term and analyzing the regularity, [43, Theorem 4.53 in Section 4.5.3] proposed the error estimate for the smooth solution and [43, Theorem 4.56 in Section 4.5.4] provided the error estimate for the low-regularity solution. If the exact solution u has uniformly continuous partial derivatives of (total) orders up to seven in each $\Omega_{p,q}$, [15, Theorem 3.1] theoretically proved the sixth-order convergence rate by the discrete maximum principle for the FDMs in [15, Theorems 2.1-2.3]. However, to the best of our knowledge, no FDMs have been presented in the literature that can theoretically establish the proof of the convergence rate for the model problem (1.1) with $u \in H^{1+\lambda}(P_\Omega)$ and $0 < \lambda < 1$.

In Example 1, the domain Ω contains only 4 subdomains, the coefficient function a exhibits high jumps, and the zero Dirichlet boundary condition is imposed. The boundary effect possibly causes the solution u to be smooth in each subdomain (see Fig. 6), leading to the numerical second-order convergence rates presented in Table 1. In the other 6 examples, we increase the frequency of the coefficient a . The discontinuities at intersection points that are far from the boundary may result

in the solution u losing regularity such that the numerical convergence rates of FEM or FDM are relatively small in Tables 2 to 7.

From the performance of FEM and FDM in Tables 4 to 6 of Examples 4 to 6, we can observe that the convergence rates of FEM are greater than those of FDM. The reason may be that the coefficient functions contain both high frequencies and large jumps in Examples 4 to 6 such that $u \in H^{1+\lambda}(P_\Omega)$ with a small λ . Another possible reason is that the FDM scheme does not include the intersection grid point (see Figs. 4 and 5), i.e., the $(u_h^D)_{i,j}$ at the intersection grid point (x_i, y_j) is ignored.

5. CONCLUSION

In this paper, we apply second-order finite element method (FEM) and finite difference method (FDM) to numerically solve elliptic cross-interface problems (1.1) with piecewise constant coefficients, homogeneous jump conditions, continuous source terms, and Dirichlet boundary conditions. The numerical results reveal interesting phenomena:

- When the coefficient functions only exhibit minor jumps or low-frequency oscillations, the numerical solutions obtained from FEM and FDM are similar (see Figs. 6 to 8).
- In contrast, when solving (1.1) with high-contrast and high-frequency coefficient functions, FEM and FDM produce markedly different solutions (see Figs. 9 to 12).

To the best of our knowledge, there is currently no literature that has revealed such distinct differences in the numerical solutions obtained from finite element and finite difference methods. These findings are particularly relevant in the context of the SPE10 benchmark problem, which contains high-contrast and high-frequency permeability resulting from the complicated geological structure in porous media. This discrepancy between FEM and FDM solutions should be carefully considered, especially when developing multiscale methods where reference solutions are often obtained by the standard FEM. We provide all necessary details to facilitate the replication of our numerical results which allows readers to easily verify the accuracy of our observations.

We only find these interesting numerical results in this paper and do not theoretically determine the reason or provide the rigorous analysis. We can only conclude that the standard FEM and FDM are insufficient to obtain the solution when the coefficient function a includes high jumps and high frequencies. Therefore, it is necessary to analyze the regularity of the solution in the model problem (1.1), which features high-contrast and high-frequency coefficient functions, and to design reliable FEM and FDM schemes to provide convincing solutions.

REFERENCES

- [1] A. Ali, H. Mankad, F. Pereira, and F. S. Sousa, The multiscale perturbation method for second order elliptic equations. *Appl. Math. Comput.* **387** (2020), 125023.
- [2] T. Arbogast, Z. Tao, and H. Xiao, Multiscale mortar mixed methods for heterogeneous elliptic problems. *Contemp. Math.* **586** (2013), 9-21.
- [3] T. Arbogast and H. Xiao, A Multiscale Mortar Mixed Space Based on Homogenization for Heterogeneous Elliptic Problems. *SIAM J. Numer. Anal.* **51** (2013), 377-399.
- [4] T. Arbogast and H. Xiao, Two-level mortar domain decomposition preconditioners for heterogeneous elliptic problems. *Comput. Methods Appl. Mech. Engrg.* **292** (2015), 221-242.
- [5] M. Blumenfeld, The regularity of interface-problems on corner-regions. *Lecture Notes in Math.* **1121** (1985), 38-54.
- [6] R. Butler, T. Dodwell, A. Reinartz, A. Sandhu, R. Scheichl, and L. Seelinger, High-performance dune modules for solving large-scale, strongly anisotropic elliptic problems with applications to aerospace composites. *Comput. Phys. Commun.* **249** (2020), 106997.
- [7] Z. Cai and S. Kim, A finite element method using singular functions for the Poisson equation: corner singularities. *SIAM J. Numer. Anal.* **39** (2001), no. 1, 286-299.
- [8] Z. Chen and S. Dai On the efficiency of adaptive finite element methods for elliptic problems with discontinuous coefficients. *SIAM J. Sci. Comput.* **24** (2002), 443-462.
- [9] X. Chen, X. Feng, and Z. Li, A direct method for accurate solution and gradient computations for elliptic interface problems. *Numer. Algorithms.* **80** (2019), 709-740.
- [10] B. Dong, X. Feng, and Z. Li, An FE-FD method for anisotropic elliptic interface problems. *SIAM J. Sci. Comput.* **42** (2020), B1041-B1066.

- [11] C. Engwer, P. Henning, A. Målqvist, and D. Peterseim, Efficient implementation of the localized orthogonal decomposition method. *Comput. Methods Appl. Mech. Engrg.* **350** (2019), 123-153.
- [12] R. Ewing, Z. Li, T. Lin, and Y. Lin, The immersed finite volume element methods for the elliptic interface problems. *Math. Comput. Simul.* **50** (1999), 63-76.
- [13] Q.W. Feng, B. Han, and M. Michelle, Sixth-order compact finite difference method for 2D Helmholtz equations with singular sources and reduced pollution effect. *Commun. Comput. Phys.* **34** (2023), 672-712.
- [14] Q.W. Feng, B. Han, and P. Minev, Sixth order compact finite difference schemes for Poisson interface problems with singular sources. *Comput. Math. Appl.* **99** (2021), 2-25.
- [15] Q.W. Feng, B. Han, and P. Minev, Compact 9-point finite difference methods with high accuracy order and/or M-Matrix property for elliptic cross-interface problems. *J. Comput. Appl. Math.* **428** (2023), 115151.
- [16] Q.W. Feng, B. Han, and P. Minev, Sixth-order hybrid finite difference methods for elliptic interface problems with mixed boundary conditions. *J. Comput. Phys.* **497** (2024) 112635.
- [17] H. Feng and S. Zhao, A fourth order finite difference method for solving elliptic interface problems with the FFT acceleration. *J. Comput. Phys.* **419** (2020), 109677.
- [18] G. J. Fix, S. Gulati and G. I. Wakoff, On the use of singular functions with finite element approximations. *J. Comput. Phys.* **13** (1973), 209-228.
- [19] S. Fu, E. Chung, and G. Li, Edge multiscale methods for elliptic problems with heterogeneous coefficients. *J. Comput. Phys.* **396** (2019), 228-242.
- [20] Y. Gong, B. Li, and Z. Li, Immersed-interface finite-element methods for elliptic interface problems with nonhomogeneous jump conditions. *SIAM J. Numer. Anal.* **46** (2008), 472-495.
- [21] R. T. Guiraldello, R. F. Ausas, F. S. Sousa, F. Pereira, and G. C. Buscaglia, Interface spaces for the Multiscale Robin Coupled Method in reservoir simulation. *Math. Comput. Simul.* **164** (2019), 103-119.
- [22] X. He, T. Lin, and Y. Lin, Immersed finite element methods for elliptic interface problems with non-homogeneous jump conditions. *Int. J. Numer. Anal. Model.* **8** (2011), 284-301.
- [23] F. Hellman and A. Målqvist, Contrast independent localization of multiscale problems. *SIAM Multiscale Model. Simul.* **15** (2017), 1325-1355.
- [24] T. Y. Hou, F. N. Hwang, P. Liu, and C. C. Yao, An iteratively adaptive multi-scale finite element method for elliptic PDEs with rough coefficients. *J. Comput. Phys.* **336** (2017), 375-400.
- [25] A. Jaramillo, R. T. Guiraldello, S. Paz, R. F. Ausas, F. S. Sousa, F. Pereira, and G. C. Buscaglia, Towards HPC simulations of billion-cell reservoirs by multiscale mixed methods. *Comput. Geosci.* **26** (2022), 481-501.
- [26] R. B. Kellogg, Singularities in interface problems. *Numerical Solution of Partial Differential Equations-II* (1971), 351-400.
- [27] R. B. Kellogg, Higher order singularities for interface problems. *The Mathematical Foundations of the Finite Element Method with Applications to Partial Differential Equations* (1972), 589-602.
- [28] R. B. Kellogg, On the Poisson equation with intersecting interfaces. *Appl. Anal.* **4** (1975), no. 2, 101-129.
- [29] S. Kim, Z. Cai, J. Pyo and S. Kong, A finite element method using singular functions: interface problems. *Hokkaido Math. J.* **36** (2007), no. 4, 815-836.
- [30] S. Kim and S. Kong, A finite element method dealing the singular points with a cut-off function. *J. Appl. Math. Comput.* **21** (2006), no. 1-2, 141-152.
- [31] V. Kippe, J. E. Aarnes, and K. A. Lie, A comparison of multiscale methods for elliptic problems in porous media flow. *Comput. Geosci.* **12** (2008), 377-398.
- [32] R. J. Leveque and Z. Li, The Immersed interface method for elliptic equations with discontinuous coefficients and singular sources. *SIAM J. Numer. Anal.* **31** (1994), 1019-1044.
- [33] Z. Li, A fast iterative algorithm for elliptic interface problems. *SIAM J. Numer. Anal.* **35** (1998), 230-254.
- [34] G. Li and J. Hu, Wavelet-based edge multiscale parareal algorithm for parabolic equations with heterogeneous coefficients and rough initial data. *J. Comput. Phys.* **444** (2021), 110572.
- [35] A. Målqvist and A. Persson, Multiscale techniques for parabolic equations. *Numer. Math.* **138** (2018), 191-217.
- [36] A. Målqvist and D. Peterseim, Localization of elliptic multiscale problems. *Math. Comput.* **83** (2014), 2583-2603.
- [37] P. Minev, S. Srinivasan, and P. N. Vabishchevich, Flux formulation of parabolic equations with highly heterogeneous coefficients. *J. Comput. Appl. Math.* **340** (2018), 582-601.
- [38] S. Nicaise, Polygonal interface problems: higher regularity results. *Commun. Partial. Differ. Equ.* **15** (1990), no. 10, 1475-1508.
- [39] S. Nicaise and A. M. Sandig, General interface problems-I. *Math. Methods Appl. Sci.* **17** (1994), 395-429.
- [40] K. Pan, D. He, and Z. Li, A high order compact FD framework for elliptic BVPs involving singular sources, interfaces, and irregular domains, *J. Sci. Comput.* **88** (2021), 1-25.
- [41] M. Petzoldt, Regularity results for Laplace interface problems in two dimensions. *J. Anal. Appl.* **20** (2001), no. 2, 431-455.
- [42] M. Petzoldt, A posteriori error estimators for elliptic equations with discontinuous coefficients. *Adv. Comput. Math.* **16** (2002), no. 1, 47-75.

- [43] D. A. Di Pietro and A. Ern, Mathematical aspects of discontinuous Galerkin methods. *Springer Berlin, Heidelberg*. 2012.
- [44] M. R. Rasaei and M. Sahimi, Upscaling and simulation of waterflooding in heterogeneous reservoirs using wavelet transformations: application to the SPE-10 model. *Transp. Porous. Med.* **72** (2008), 311-338.
- [45] P. Tahmasebi and S. Kamrava, A multiscale approach for geologically and flow consistent modeling. *Transp. Porous. Med.* **124** (2018), 237-261.
- [46] J. L. Vázquez, The Porous medium equation: mathematical theory. *Clarendon Press*. 2007.
- [47] A. Wiegmann and K. P. Bube, The explicit-jump immersed interface method: finite difference methods for PDEs with piecewise smooth solutions. *SIAM J. Numer. Anal.* **37** (2000), 827-862.
- [48] S. Yu and G. W. Wei, Three-dimensional matched interface and boundary (MIB) method for treating geometric singularities. *J. Comput. Phys.* **227** (2007), 602-632.
- [49] S. Yu, Y. Zhou, and G. W. Wei, Matched interface and boundary (MIB) method for elliptic problems with sharp-edged interfaces. *J. Comput. Phys.* **224** (2007), 729-756.
- [50] Z. Zhang, M. Ci, and T. Y. Hou, A multiscale data-driven stochastic method for elliptic PDEs with random coefficients. *SIAM Multiscale Model. Simul.* **13** (2015), 173-204.
- [51] X. Zhong, A new high-order immersed interface method for solving elliptic equations with imbedded interface of discontinuity. *J. Comput. Phys.* **225** (2007), 1066-1099.
- [52] Y. C. Zhou and G. W. Wei, On the fictitious-domain and interpolation formulations of the matched interface and boundary (MIB) method. *J. Comput. Phys.* **219** (2006), 228-246.
- [53] Y. C. Zhou, S. Zhao, M. Feig, and G. W. Wei, High order matched interface and boundary method for elliptic equations with discontinuous coefficients and singular sources. *J. Comput. Phys.* **213** (2006), 1-30.

DEPARTMENT OF MATHEMATICS, UNIVERSITY OF PITTSBURGH, PITTSBURGH, PA 15260, USA. qif21@pitt.edu

DEPARTMENT OF MATHEMATICAL AND STATISTICAL SCIENCES, UNIVERSITY OF ALBERTA, EDMONTON, ALBERTA, T6G 2G1, CANADA. qfeng@ualberta.ca